

On the origins of C IV absorption profile diversity in broad absorption line quasars

Alexei Baskin,^{1*} Ari Laor¹ and Fred Hamann²

¹*Physics Department, Technion – Israel Institute of Technology, Haifa 32000, Israel*

²*Department of Astronomy, University of Florida, Gainesville, FL 32611-2055, USA*

ABSTRACT

There is a large diversity in the C IV broad absorption line (BAL) profile among BAL quasars (BALQs). We quantify this diversity by exploring the distribution of the C IV BAL properties, FWHM, maximum depth of absorption and its velocity shift (v_{md}), using the SDSS DR7 quasar catalogue. We find the following: (i) Although the median C IV BAL profile in the quasar rest-frame becomes broader and shallower as the UV continuum slope (α_{UV} at 1700–3000 Å) gets bluer, the median individual profile in the absorber rest-frame remains identical, and is narrow (FWHM = 3500 km s^{−1}) and deep. Only 4 per cent of BALs have FWHM > 10,000 km s^{−1}. (ii) As the He II emission equivalent-width (EW) decreases, the distributions of FWHM and v_{md} extend to larger values, and the median maximum depth increases. These trends are consistent with theoretical models in which softer ionizing continua reduce overionization, and allow radiative acceleration of faster BAL outflows. (iii) As α_{UV} becomes bluer, the distribution of v_{md} extends to larger values. This trend may imply faster outflows at higher latitudes above the accretion disc plane. (iv) For non-BALQs, the C IV emission line decreases with decreasing He II EW, and becomes more asymmetric and blueshifted. This suggests an increasing relative contribution of emission from the BAL outflow to the C IV emission line as the ionizing spectral energy distribution (SED) gets softer, which is consistent with the increasing fraction of BALQs as the ionizing SED gets softer.

Key words: galaxies: active – quasars: absorption lines – quasars: general.

1 INTRODUCTION

Broad absorption line quasars (BALQs) are a subtype of quasars, characterized by the presence of broad and blueshifted absorption features (Weymann, Carswell & Smith 1981). The intrinsic fraction of quasars that are BALQs is estimated to be typically ~20 per cent (Hewett & Foltz 2003; Reichard et al. 2003; Knigge et al. 2008; Gibson et al. 2009; cf. Allen et al. 2011), and ranges from ~4 per cent in blue, strong He II emission quasars, to ~30 per cent in red, weak He II emission quasars (Baskin, Laor & Hamann 2013, hereafter BLH13). Although there are several differences in emission properties between BALQs and non-BALQs, the two subtypes appear to be drawn from the same population (Weymann et al. 1991; Hamann, Korista & Morris 1993; Reichard et al. 2003). The C IV broad absorption line (BAL) spans a large range in depth, width and the velocity shift (v_{shift}) of maximum absorption depth (v_{md}) among different BALQs.

What produces the large diversity of C IV BAL properties? The maximal outflow velocity of C IV BAL has a clear correlation with the quasar luminosity in X-ray weak objects (Brandt, Laor & Wills 2000; Laor & Brandt 2002; Gibson et al. 2009). The C IV BAL absorption is on average stronger in BALQs that also show lower ionization BALs (Reichard et al. 2003; Filiz Ak et al. 2014). Recently, BLH13 studied the median absorption properties of BALQs, and found that the width and v_{shift} of C IV BAL are set by the He II $\lambda 1640$ emission equivalent-width (EW), while the BAL depth is controlled by the UV continuum slope in the 1700–3000 Å range (α_{UV}). The explored BAL profiles in BLH13 are *median* profiles, derived from composite spectra of BALQs from the Sloan Digital Sky Survey (SDSS; York et al. 2000) Data Release 7 (DR7; Abazajian et al. 2009; Schneider et al. 2010; Shen et al. 2011).

In this paper, we extend the study of BLH13, and explore the dependence of the C IV BAL profile on the He II EW and α_{UV} for *individual* absorption features in BALQs from the same SDSS DR7 sample ($1.75 \leq z \leq 2.05$). We find that in contrast with the median C IV BAL profiles which have FWHM > 5000 km s^{−1}, the individual profiles are

* E-mail: alexei@physics.technion.ac.il

rather narrow with a median FWHM = 3500 km s⁻¹. We also find that α_{UV} has a significantly weaker effect on the BAL depth, and that the He II EW has a weaker effect on the BAL FWHM, compared to the effects implied by the median profiles in BLH13. As we show below, these differences result from the strong dependence of v_{md} on both α_{UV} and the He II EW.

The motivation to use the He II EW and α_{UV} is driven by both observational and theoretical considerations (see BLH13 for a more extensive discussion). Observationally, BALQs are reported to have a weaker He II EW (Richards et al. 2002; Reichard et al. 2003) and a redder α_{UV} compared to non-BALQs (Reichard et al. 2003; Maddox et al. 2008; Gibson et al. 2009; Allen et al. 2011). Theoretically, the EW of the He II $\lambda 1640$ recombination line is a measure of the continuum strength above 54 eV, compared to the near-UV continuum, and thus is indicative of the hardness of the ionizing spectral energy distribution (SED). The UV slope is reported to correlate with other reddening indicators (e.g. Baskin & Laor 2005; Stern & Laor 2012), and is potentially indicative of our viewing angle, with objects observed closer to edge-on having a redder α_{UV} (BLH13). BLH13 show that a Small Magellanic Cloud extinction law with $A_V = 0.06$ mag can explain the median reddening of BALQs compared to non-BALQs in a large range of $\lambda_{\text{rest}} = 1000 - 3000$ Å, further supporting the interpretation of α_{UV} as a dust-reddening indicator.

The paper is structured as follows: In Section 2, we describe the data analysis method. The results are presented in Section 3 and discussed in Section 4. Section 5 summarizes our conclusions.

2 THE DATA ANALYSIS

A complete description of the sample and the data analysis is provided in BLH13, and is briefly reviewed here. The data set is drawn from the SDSS DR7 quasar catalogue of Shen et al. (2011). In this catalogue, the BALQ classification is based on the Gibson et al. (2009) BALQ catalogue for objects that are included in the SDSS DR5, and on a visual inspection of the C IV region for the remaining $\simeq 20$ per cent of objects. An object is flagged as a BALQ by Gibson et al. (2009), if it has $\text{BI}_0 > 0$, where BI_0 is a modified version of ‘balnicity index’ (BI; Weymann et al. 1991). For BI_0 , the integration over the normalized f_λ starts at $v_{\text{shift}} = 0$, rather than at -3000 km s⁻¹ which is used for BI. We require the spectra to be in the $1400 \leq \lambda_{\text{rest}} \leq 3000$ Å range, i.e. $1.75 \leq z \leq 2.05$ for the SDSS, which allows to cover the C IV BAL and $\lambda_{\text{rest}} = 3000$ Å that is used for α_{UV} , and to exclude LoBALQs using Mg II. This criterion produces a sample of 1691 BALQs and 13,388 non-BALQs. We further require the objects to have a signal-to-noise ratio $S/N \geq 3$ in the SDSS i -filter, to avoid unusually low-S/N spectra, which excludes 39 BALQs and 739 non-BALQs. Finally, we exclude 56 LoBALQs with a Mg II BAL detection (Shen et al. 2011), and construct a sample of HiBALQs only. The final data set is comprised of 1596 HiBALQs and 12,649 non-BALQs.

It has been suggested that radio-loud (RL) BALQs have different BAL properties than radio-quiete (RQ) BALQs (e.g. Becker et al. 1997; Brotherton et al. 1998). In contrast, Rochais et al. (2014) find that RL and RQ BALQs are not

fundamentally different objects. Here, we use the radio loudness parameter $R \equiv f_{6\text{ cm}}/f_{2500}$ provided in the Shen et al. (2011) catalogue, where $f_{6\text{ cm}}$ is estimated from the FIRST integrated flux density at 20 cm (Becker, White & Helfand 1995; White et al. 1997), assuming $f_\nu \propto \nu^{-0.5}$. Objects with $R > 10$ are classified as RL (89 BALQs and 782 non-BALQs in our sample). The fraction of RL objects is $\lesssim 10$ per cent in the BALQ and non-BALQ subsamples explored here, and thus has a little effect on our results. In the subsequent analysis, we mark RL BALQs, but do not exclude them from our sample. As we show below, RL BALQs have a preference toward a smaller He II EW and a redder α_{UV} compared to RQ BALQs, which results in a different ‘typical’ BAL profile. However, when RL and RQ BALQs are matched in the emission parameters (see also Rochais et al. 2014, where the objects are matched in L), there are no systematic differences in the C IV BAL profile between the two subclasses. This implies that radio loudness has no direct effect on the BAL properties.

The following procedure is carried out for each object (both a BALQ and a non-BALQ):

(i) The spectrum is smoothed by a 22 pixel-wide moving average filter, which is equivalent to $\simeq 1350$ km s⁻¹ (i.e. ~ 9 resolution elements; York et al. 2000). This relatively broad filter smooths out any narrow features ($\lesssim 500$ km s⁻¹) superimposed on the C IV BAL, and diminishes their effect on the measurement of maximum depth of the C IV BAL (see below).

(ii) The spectrum is normalized by the mean f_λ in the $\lambda_{\text{rest}} = 1700 - 1720$ Å range.

(iii) The He II emission EW is measured by integrating the normalized f_λ in the $\lambda_{\text{rest}} = 1620 - 1650$ Å range, and approximating f_λ^{cont} by a constant value of 1 between the normalization window and 1620 Å. This rough approximation of f_λ^{cont} does not affect significantly our results (see BLH13).

(iv) The UV spectral slope α_{UV} ($f_\nu \propto \nu^{\alpha_{UV}}$) is measured between the 1700–1720 and 2990–3010 Å windows, using the mean f_λ of each window. The accuracy of α_{UV} is affected by the flux calibration of individual spectra. The flux is calibrated by matching the spectra of simultaneously observed standard stars to the magnitude of their point spread function, and it is accurate to a level of a few per cent for $\lambda_{\text{obs}} > 4000$ Å (Adelman-McCarthy et al. 2007, 2008). For $\lambda_{\text{obs}} < 4000$ Å, Pâris et al. (2011) report systematic excess light in the SDSS DR7 spectra (see also Abazajian et al. 2009). Since $\lambda_{\text{obs}} = 4000$ Å corresponds to $\lambda_{\text{rest}} = 1450$ Å for the lowest $z = 1.75$ of our sample, the measurement of α_{UV} is not affected by this systematic excess.

We take from the Shen et al. (2011) catalogue the values of $L(3000 \text{ Å})$, Mg II FWHM and M_{BH} , which is evaluated using the Vestergaard & Osmer (2009) prescription. We also calculate $\log L/L_{\text{Edd}} = \log L(3000 \text{ Å}) - \log M_{\text{BH}} - 37.4$, where we use a bolometric correction factor of 5.15 from Shen et al. (2008).

The objects are binned based on the He II EW and α_{UV} , into four bins for each parameter. The binning is such that each BALQ bin contains the same number of objects. The matching non-BALQ bins cover the same parameter range, but do not have equal number of objects per bin. Fig. 1 presents the distribution of α_{UV} versus the He II EW for the

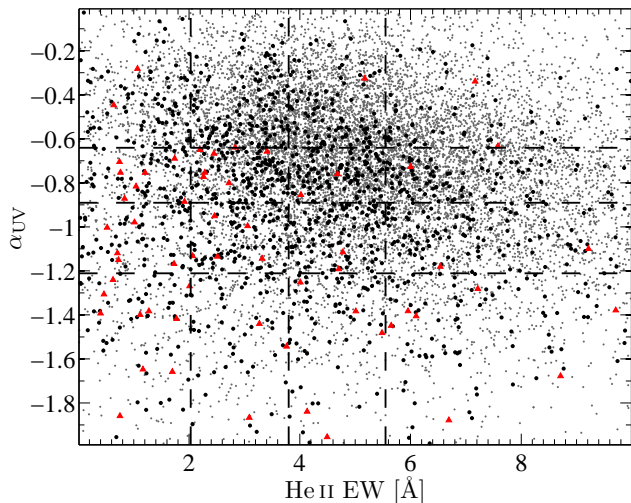


Figure 1. The distribution of α_{UV} versus the He II EW for the sample of BALQs (large black dots for RQ and red triangles for RL) and non-BALQs (small grey dots) which are used in this study. The dashed lines are the boundaries that define the four He II EW bins and the four α_{UV} bins.

whole sample of BALQs and non-BALQs, and the boundaries that are used to define the bins. The He II EW and α_{UV} distributions for BALQs and non-BALQs within each bin can be somewhat different, but the difference in the median value of the parameter that is used for binning is below 10 per cent within each bin for all bins (Tables 2 and 3). There is no correlation between the He II EW and α_{UV} in BALQs, and a very weak correlation in non-BALQs. The Spearman rank-order correlation coefficient is $r_s = -0.007$ and -0.139 for BALQs and non-BALQs, respectively. Note that RL BALQs (Fig. 1, red triangles) have a preference toward lower values of He II EW and a red α_{UV} .

We measure the maximum absorption depth (CF), velocity shift of the maximum absorption depth (v_{md}) and the FWHM for the deepest C IV BAL trough of each BALQ. For brevity, we denote the maximum absorption depth as CF, noting that this notation is formally correct (i.e. implies the covering factor) only if $\tau(v_{md}) \gg 1$. The v_{md} is measured directly for each BALQ spectrum, and equals the value of v_{shift} where $f_\lambda(\lambda_{rest})$ is minimal, with the requirement that $0 < v_{shift} < 30,000 \text{ km s}^{-1}$. The value of v_{shift} is calculated relative to $\lambda = 1549 \text{ \AA}$. The value of CF and the FWHM is estimated as follows:

- (i) A non-BALQ composite is calculated for all the non-BALQ bins (based on the He II EW and α_{UV}).¹ This composite is assumed to represent the intrinsically unabsorbed emission for the BALQs which reside in that bin.
- (ii) Each BALQ spectrum is divided by the non-BALQ composite.
- (iii) A power law is fit between 1600 and 1800 \AA , and

is extrapolated to $\lambda_{rest} < 1600 \text{ \AA}$ (using the 1700–3000 \AA range for the fit produces similar results).

(iv) The ratio spectrum [from step (ii)] is divided by the power law [from step (iii)], and the result is adopted as the emission-corrected absorption spectrum.

(v) The absorption depth at v_{md} is adopted as the CF.

(vi) Starting from v_{md} , we search for the closest $v_{shift} > v_{md}$ and $v_{shift} < v_{md}$, where the absorption depth is half of that adopted in step (v). The FWHM is the difference between these two values of v_{shift} .

Measuring v_{md} from the emission-corrected absorption spectrum, i.e. after steps (i)–(iv), rather than from the observed spectrum, does not change qualitatively the resulting trends which are explored below. The assumption in step (i) produces ≈ 10 BALQs per bin with CF smaller than 0.1, which corresponds to BI = 0 (i.e. formally not a BALQ). However, we retain these BALQs in our BALQ sample, since reclassifying the objects of the SDSS DR7 quasar catalogue of Shen et al. (2011) is beyond the scope of our paper. Excluding these BALQs from the BALQ sample does not affect our results.

As shown in BLH13, the selection by the He II EW provides a well-matched C IV emission profile on the red side for BALQs and non-BALQs. The selection by α_{UV} produces a BALQ/non-BALQ ratio spectrum with a weak pseudo-absorption at a level of $\lesssim 0.05$ for $v_{shift} \gtrsim 0$. A mismatch in the C IV emission profile has a very small effect on the measurement of BALs with $v_{md} > 10^4 \text{ km s}^{-1}$, since the C IV emission is generally found at $v_{shift} < 10^4 \text{ km s}^{-1}$. As we show below, the BALs with $v_{md} < 10^4 \text{ km s}^{-1}$ tend to have a CF > 0.5 that is well above 0.05. Thus, we neglect the effect of pseudo-absorption. We cannot test whether there are significant differences on the blue side, which will affect the emission-corrected absorption spectrum.

Table 1 lists the measured He II EW, α_{UV} and the C IV BAL parameters for individual objects.² Specifically, column (1) lists the SDSS DR7 designation (J2000.0). Columns (2) and (3) provide the right ascension and declination angles (in decimal degrees; J2000.0). Column (4) lists the values of z from Hewett & Wild (2010) which are used in this study. Columns (5) and (6) list the measured values of He II EW (in \AA) and α_{UV} . Column (7) provides v_{md} of C IV BAL in units of km s^{-1} . Columns (8) and (9) list the C IV BAL CF and FWHM (in km s^{-1}) for the He II-EW binning. Binning by α_{UV} procedures slightly different C IV BAL CF and FWHM for some objects (the measurement of v_{md} is independent of the binning; see above). However, there is a very good overall agreement between the two binning procedures. Comparing the values of CF from the two procedures yields a Pearson linear-correlation coefficient of $r_P = 0.997$. A similar analysis for the FWHM produces $r_P = 0.961$.

Tables 2 and 3 summarize the median properties of the He II EW and α_{UV} bins, respectively. The tables also provide the median $L(3000\text{\AA})$, Mg II FWHM, M_{BH} and L/L_{Edd} for each bin. The bins are similar in these properties. All bins have a roughly the same $L(3000\text{\AA}) \approx 10^{46} \text{ erg s}^{-1}$, and a similar $M_{BH} \approx 10^9 M_\odot$ within a range of $\approx \pm 0.1$ dex. The

¹ We use a modified median method to calculate the composites. In this method, the adopted value for the composite f_λ at a given λ_{rest} equals to the mean f_λ of 10 per cent of the objects above and below the median (i.e. 20 per cent of objects in total; see BLH13 for details).

² The full version of Table 1 is available online in a machine readable format.

Table 1. Measured emission and absorption properties.^a

SDSS J	R.A.	Dec.	z	He II EW	α_{UV}^b	v_{md}	CF ^c	FWHM ^c
	(deg)	(deg)		(Å)		(km s ⁻¹)		(km s ⁻¹)
(1)	(2)	(3)	(4)	(5)	(6)	(7)	(8)	(9)
000013.80–005446.8	0.057506	−0.91300	1.8409	6.8	−1.00	2277	0.73	1932
000038.66+011426.2	0.161080	1.24060	1.8330	6.1	−1.39	7107	0.93	4899
000119.64+154828.8	0.331840	15.80800	1.9211	3.3	−1.18	8418	0.78	10695
000645.98–004840.1	1.691600	−0.81116	2.0036	7.8	−0.93	16905	0.25	1794
000653.31+000135.7	1.722100	0.02660	1.9481	5.5	−0.66	5382	0.85	4554

^a The full table is available online in a machine readable format.

^b Measured between 1710 and 3000 Å ($f_\nu \propto \nu^\alpha$).

^c The values of CF and FWHM are from the He II EW binning of the median non-BALQ emission. Binning by α_{UV} yields nearly identical results (see text).

median L/L_{Edd} is large (>0.3) in all bins, and spans a range of $\simeq 0.2$ dex.

Tables 2 and 3 also list the number of RL quasars (N_{RL}) in each bin. The observed fraction of RL BALQs from the total RL quasar population increases with decreasing He II EW and a redder α_{UV} . For the He II EW, the fraction increases from 4 per cent (15/394) to 28 per cent (43/151) from the highest to the lowest bin. For α_{UV} , the fraction increases from 4 per cent (9/258) to 21 per cent (48/229) from the bluest to the reddest bin. The RQ population shows a similar increase, from 7 per cent (384/5335) to 22 per cent (356/1616) for the He II-EW binning, and from 7 per cent (390/5555) to 21 per cent (351/1696) for the α_{UV} binning.

2.1 Alternative HiBALQ samples

We explore the effect of using only BALQs from the Gibson et al. (2009) catalogue, where all BALQs are identified by an automated procedure, unlike the Shen et al. (2011) catalogue (see above). There are 1287 HiBALQs in the Gibson et al. (2009) catalogue which comply to our selection criteria.³ This subsample of 1287 HiBALQs produces similar results to the whole sample of 1596 HiBALQs, both qualitatively and quantitatively.

We also check the effect of a subsample that includes only BALQs with a reported BI > 0 (Gibson et al. 2009), which is a more ‘traditional’ criterion of BALQ identification compared to BI₀ > 0 . The subsample contains 1046 HiBALQs, and produces similar trends to the whole HiBALQ sample. There are two main quantitative differences between the BI > 0 subsample and the whole sample. First, the BI > 0 subsample implies median values of v_{md} which are ~ 1000 km s⁻¹ larger. This is expected since the BI > 0 criterion does not identify BALs in the $0 < v_{shift} < 3000$ km s⁻¹ range, in contrast with the BI₀ > 0 criterion (see above). Second, a more marginal difference is that the BI > 0 subsample has median values of FWHM which are larger by 0–600 km s⁻¹ than for the whole sample (the difference in the median value between the two samples with all bins combined is 200 km s⁻¹). Using the Shen et al. (2011) sample,

with BALQs detected by a visual inspection, allows us to examine trends across a wider range of outflow properties.

3 RESULTS

3.1 Distribution of the profile properties of C IV BAL

Figure 2 presents the distribution of FWHM versus v_{md} of the C IV BAL for the 4×4 He II EW and α_{UV} bins. The BALQ and non-BALQ samples are first binned into four α_{UV} bins, and then each α_{UV} bin is binned into four bins based on the He II EW. For a given He II EW bin, v_{md} reaches larger values as α_{UV} becomes bluer, while the range of FWHM values remains approximately constant with α_{UV} . For a given α_{UV} bin, both v_{md} and the FWHM reach larger values as the He II EW becomes weaker. The overall trend is that BALs cluster at the lowest values of v_{md} and FWHM in the reddest- α_{UV} highest-He II EW bin (top-right panel), while BAL values are rather evenly spread in the bluest- α_{UV} weakest-He II EW bin (bottom-left panel). This trend is further explored below. For all bins, the FWHM is typically smaller than v_{md} for $v_{md} > 4000$ km s⁻¹, except the 4×1 reddest α_{UV} bins (the rightmost panels in Fig. 2).

Figure 3 presents a histogram of the distribution of v_{md} values. The left panels present the distribution in each He II EW bin. In all bins, the distribution has a peak at $v_{md} < 5000$ km s⁻¹. As the He II EW becomes weaker, the distribution becomes flatter, and the median value of v_{md} increases from 5200 km s⁻¹ for the highest He II EW bin to 8000 km s⁻¹ for the lowest one (Table 2). The right panels of Fig. 3 present the distribution of v_{md} in each α_{UV} bin. Here, the distribution becomes flatter as α_{UV} becomes bluer. The median value of v_{md} increases from 4500 km s⁻¹ for the reddest bin to 8700 km s⁻¹ for the bluest α_{UV} bin (Table 3). The median value of v_{md} for the whole BALQ sample is 6500 km s⁻¹.

Figure 4 presents the distribution of FWHM values of the C IV BAL. The left panels present the distribution in each He II EW bin. For all bins, the distribution decreases sharply with increasing FWHM for FWHM $\gtrsim 3000$ km s⁻¹, and the decrease is sharper for a higher He II EW. To quantify the decrease, we fit a power-law in the range FWHM = 2000–10,000 km s⁻¹ for the two weaker bins, and between 2000–8000 km s⁻¹ for the two stronger bins, which have a

³ The fraction of HiBALQs from the Gibson et al. (2009) catalogue out of our whole HiBALQ sample is 1287/1596 $\simeq 80$ per cent, which is similar to the fraction of BALQs from Gibson et al. (2009) out of the whole BALQ sample of Shen et al. (2011).

Table 2. The median properties of the He II EW binned objects.

Class	N_{bin}	N_{obj}	He II EW (Å)	α_{UV}^a	log $L(3000\text{Å})$ (erg s^{-1})	Mg II FWHM (km s^{-1})	log M_{BH} (M_{\odot})	log L/L_{Edd}	N_{RL}	CF	C IV BAL ^b v_{md} (km s^{-1})	FWHM (km s^{-1})
BALQs	1	399	7.0	−0.97	45.90	3900	9.03	−0.48	15	0.73	5200	3000
	2	399	4.7	−0.83	45.97	4400	9.14	−0.52	12	0.71	6200	3300
	3	399	3.0	−0.79	46.00	4100	9.09	−0.44	19	0.75	7300	3700
	4	399	0.9	−0.96	45.99	3400	8.93	−0.30	43	0.80	8000	4300
non-	1	5330	7.3	−0.77	45.81	3800	8.93	−0.49	379			
BALQs	2	3461	4.7	−0.65	45.93	4000	9.03	−0.47	146			
	3	2425	3.1	−0.61	45.94	3700	8.98	−0.38	147			
	4	1368	1.0	−0.69	45.93	3300	8.87	−0.30	108			

^a Measured between 1710 and 3000 Å ($f_{\nu} \propto \nu^{\alpha}$).^b The median value of individual BAL profiles (cf. BLH13, where the tabulated values are for the median BAL profile).**Table 3.** The median properties of the α_{UV} binned objects.^a

Class	N_{bin}	N_{obj}	α_{UV}	He II EW (Å)	log $L(3000\text{Å})$ (erg s^{-1})	Mg II FWHM (km s^{-1})	log M_{BH} (M_{\odot})	log L/L_{Edd}	N_{RL}	CF	C IV BAL ^b v_{md} (km s^{-1})	FWHM (km s^{-1})
BALQs	1	399	−0.48	3.5	45.92	4100	9.08	−0.49	9	0.69	8700	3500
	2	399	−0.76	4.0	45.97	4100	9.09	−0.45	17	0.69	7700	3600
	3	399	−1.05	4.3	45.97	3900	9.05	−0.41	15	0.76	5700	3500
	4	399	−1.51	3.5	46.00	3600	9.02	−0.38	48	0.82	4500	3300
non-	1	5414	−0.44	4.6	45.86	3800	8.96	−0.46	249			
BALQs	2	3334	−0.76	5.4	45.92	3800	8.99	−0.43	174			
	3	2349	−1.02	5.9	45.89	3700	8.97	−0.42	171			
	4	1526	−1.45	5.1	45.86	3600	8.92	−0.41	181			

^a Measured between 1710 and 3000 Å ($f_{\nu} \propto \nu^{\alpha}$).^b The median value of individual BAL profiles (cf. BLH13, where the tabulated values are for the median BAL profile).

negligible number of objects with $\text{FWHM} > 8000 \text{ km s}^{-1}$. The slope of the power-law decreases monotonically from −1.1 for the weakest He II EW bin, through −1.8 and −2.0, to −2.5 for the strongest one. The median value of FWHM increases from 3000 km s^{-1} for the strongest He II EW bin to 4300 km s^{-1} for the weakest bin (see Table 2). The right panels of Fig. 4 present the FWHM distribution in each α_{UV} bin. The distribution is independent of α_{UV} , as manifested by both the similar slopes (−2.2 to −2.5; Fig. 4), and the similar median FWHM of $\simeq 3500 \text{ km s}^{-1}$ for all α_{UV} bins (Table 3). We also measure the velocity dispersion of the individual C IV BAL absorption profiles, and its distributions show similar trends with the He II EW and α_{UV} , as found above for the FWHM. The median FWHM of the whole BALQ sample is 3500 km s^{-1} . Only $\simeq 4$ per cent of objects have a C IV BAL with $\text{FWHM} > 10,000 \text{ km s}^{-1}$, as seen in the BALQ PHL 5200 (Junkkarinen, Burbidge & Smith 1983), which is often perceived as the ‘prototype’ BALQ (e.g. Turnshek et al. 1988).

Figure 5 presents the distribution of the C IV BAL CF. The CF distribution can be represented as being composed of two components. The first component, which is roughly similar for all bins, increases from $\text{CF} = 0$ as $\propto \text{CF}^{1.6}$ (we fit a power-law in the range of $\text{CF} = 0.5\text{--}0.8$), and peaks at $\text{CF} \approx 0.9$. The second component is an excess of objects

in the $\text{CF} \approx 0.2\text{--}0.4$ range relative to the first component. This excess increases as the He II EW becomes stronger, and as α_{UV} becomes bluer (Fig. 5). The excess has a little effect on the median CF which increases slightly from $\simeq 0.7$ to $\simeq 0.8$ as α_{UV} becomes redder and as the He II EW decreases. The excess has only a minor effect on the overall shape of the CF distribution for the He II EW binning, and the difference among the He II EW bins is statistically insignificant for most bin pairs (see below).

Figure 6 presents CF versus v_{md} of the individual profiles for the highest and the lowest He II EW bins. The typical CF decreases as v_{md} increases. A physical interpretation of this trend is presented in Section 4.

3.1.1 Statistical tests

Table 4 lists the values of r_s for correlations between the C IV BAL properties and the He II EW and α_{UV} . These values suggest that v_{md} is more strongly controlled by α_{UV} than by the He II EW ($r_s = 0.30$ vs. -0.15); the FWHM depends on the He II EW, and is independent of α_{UV} ($r_s = -0.23$ and 0.03 , respectively); and the CF has a slightly tighter correlation with α_{UV} than with the He II EW, although both correlations are rather loose ($r_s = -0.17$ vs. -0.13). Table 4 also lists the values of r_s for the relations between the different

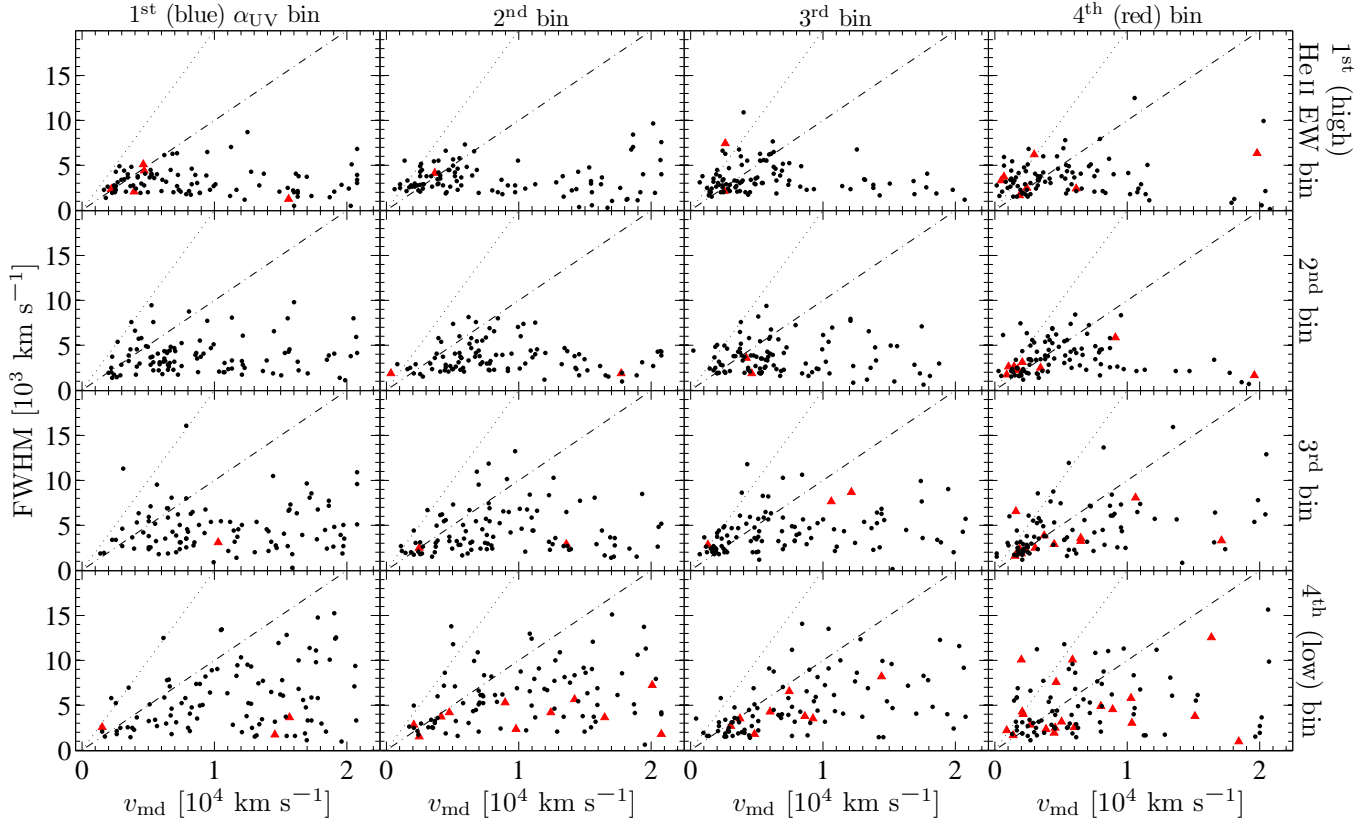


Figure 2. The distribution of FWHM versus v_{md} of the C IV BAL, for the He II EW and α_{UV} bins. The BALQ and non-BALQ samples are first binned into α_{UV} bins, and then each α_{UV} bin is binned based on the He II EW. RL BALQs are denoted by a red triangle. The slope decreases (i.e. becomes redder) from left to right, and the He II EW decreases from top to bottom. The dot-dashed line and the dotted line denote 1:1 and 2:1 relation, respectively. Note the trend where in the reddest- α_{UV} highest-He II EW bin, BALs cluster at the lowest values of v_{md} and FWHM (most right-top panel), while in the bluest- α_{UV} weakest-He II EW bin, BAL values are rather evenly spread (most left-bottom panel).

BAL properties. These values slightly depend on whether the BAL properties are derived using a non-BALQ composite matched in the He II EW or in α_{UV} (Section 2). We list r_s for both matchings. There is a strong anti-correlation ($r_s \simeq -0.53$) between v_{md} and CF, implying a decrease in CF with increasing v_{md} (see also Fig. 6). The FWHM and CF have a positive correlation ($r_s \simeq 0.34$). The correlation between v_{md} and the FWHM is small ($r_s \simeq 0.22$).

We have applied the Kolmogorov-Smirnov (K-S) test to quantify the strength of the differences among distributions for the He II EW and α_{UV} binning, for the three BAL parameters (Figs 3–5). For v_{md} , the difference is statistically significant for most bin pairs (p -value < 0.01 ; with $p < 10^{-4}$ in most cases). The three exceptions are the first (bluest) α_{UV} bin compared to the second one ($p = 0.09$), and the third He II EW bin compared to the fourth (lowest) and the second one ($p = 0.15$ and 0.02 , respectively). For the FWHM, the difference is statistically significant for all He II EW bin pairs ($p < 10^{-5}$ in most cases), except for the first bin compared to the second one ($p = 0.15$). The difference is statistically insignificant for all α_{UV} bin pairs ($p > 0.55$). For the CF, the distribution for the He II EW binning is different with a high statistical significance only for the fourth bin compared to the other three ($p < 10^{-3}$; $p > 0.05$ for other bin pairs). For the α_{UV} binning, the difference in CF distri-

Table 4. The Spearman rank-order correlation coefficient (r_s) for the C IV BAL properties.^{a, b}

	v_{md}	FWHM	CF
He II EW	−0.153	−0.225	−0.125
α_{UV}	0.301	0.032	−0.171
v_{md}		0.216	−0.529
FWHM	0.158		0.336
CF	−0.548	0.353	

^a The null probability is $p < 10^{-6}$ for all relations, except the relation of FWHM with α_{UV} for which $p = 0.2$.

^b The values of r_s for correlations among BAL properties slightly depend on whether the properties are derived using a non-BALQ composite matched in the He II EW or in α_{UV} (Section 2). The values above the diagonal are for matching in the He II EW, and those below are for matching in α_{UV} .

bution is statistically significant for all bin pairs ($p < 10^{-2}$), except the first compared to the second bin ($p = 0.45$).

The RL and RQ BALQ populations have a different distribution of the He II EW and α_{UV} (K-S test yields $p \approx 10^{-6}$ and 10^{-9} , respectively). RL BALQs have smaller values of He II EW and redder α_{UV} . The median He II EW is 3.9 and 2.2 Å for RQ and RL BALQs, respectively. The median α_{UV}

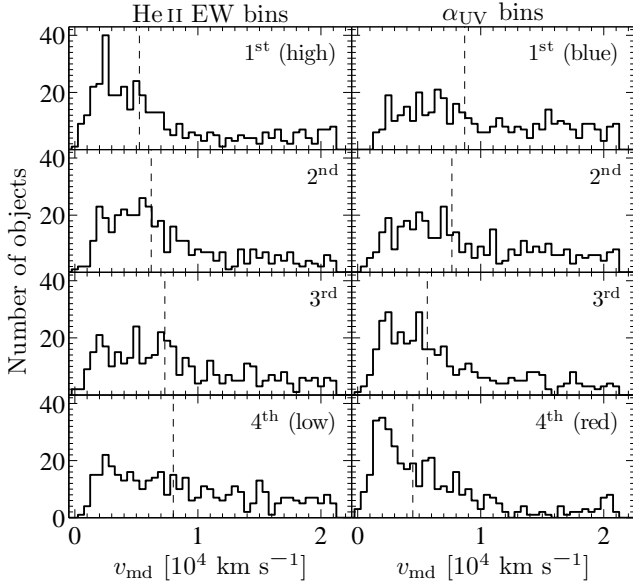


Figure 3. The distribution of v_{md} of C IV BAL in each He II EW and α_{UV} bin. The median v_{md} of the bin is denoted by the vertical dashed line. There are more C IV BALs with high v_{md} ($\gtrsim 10^4 \text{ km s}^{-1}$) as the He II EW decreases (left panels), and as α_{UV} becomes bluer (right panels).

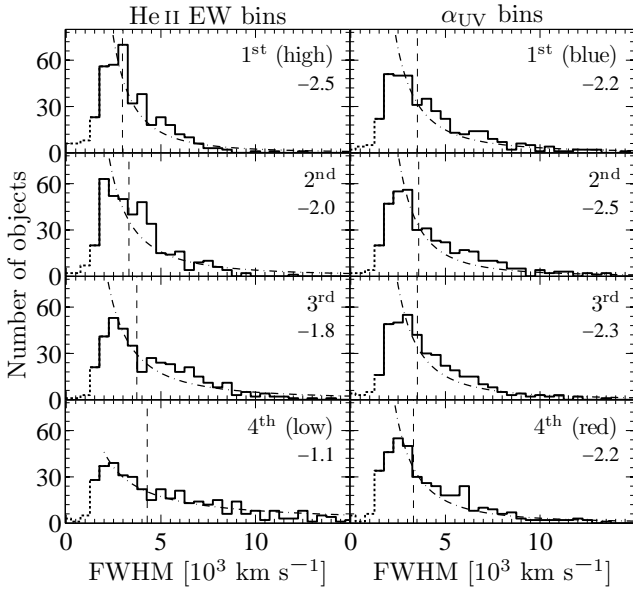


Figure 4. The same as Fig. 3, for the FWHM of C IV BAL. The dotted line marks the distribution for $\text{FWHM} < 1500 \text{ km s}^{-1}$, i.e. smaller than the width of the smoothing filter that is applied to object spectra. The dot-dashed line is a power-law fit, which slope is denoted in the panel (see text). For all bins, the median $\text{FWHM} \lesssim 4000 \text{ km s}^{-1}$, and the distribution falls off significantly by $\text{FWHM} \gtrsim 10,000 \text{ km s}^{-1}$. There are more C IV BALs with $\text{FWHM} > 5000 \text{ km s}^{-1}$ as the He II EW decreases (left panels). The FWHM distribution is independent of α_{UV} (right panels).

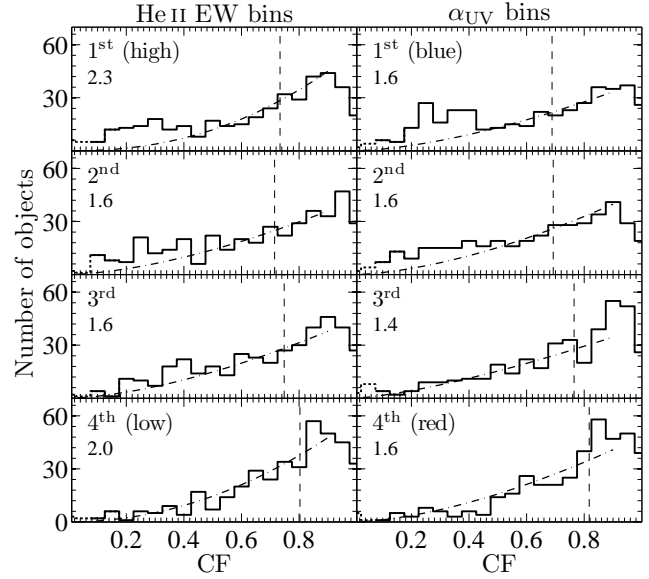


Figure 5. The same as Fig. 4, for the C IV BAL CF. The dotted line marks the distribution for BAL $\text{CF} < 0.1$, which implies $\text{BI} = 0$ (see Section 2). The power-law fit is between the CF of 0.5 and 0.8, and it has a similar slope for all bins. The excess of objects with a small value (< 0.5) of CF relative to the power-law fit increases as the He II EW becomes larger, and as α_{UV} becomes bluer.

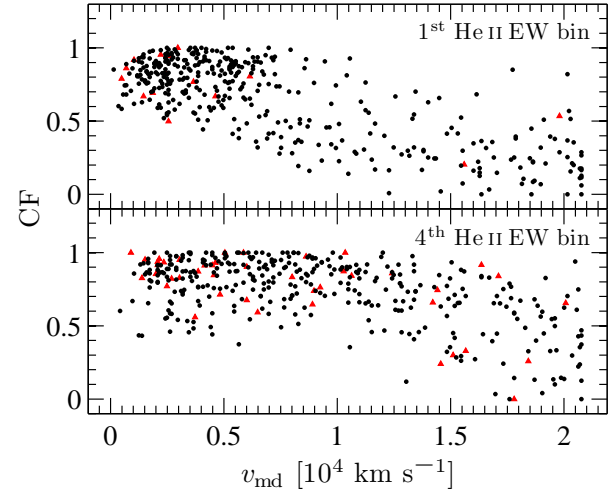


Figure 6. The C IV BAL CF versus v_{md} , for RQ (black dots) and RL (red triangles) BALQs. For all He II EW and α_{UV} bins, the CF decreases as v_{md} increases. RQ and RL BALQs show a similar distribution. We present only the highest and the lowest He II EW bins, for brevity.

is -0.88 for RQ BALQs and -1.26 for RL BALQs. The distribution of the C IV BAL FWHM and CF is similar for both populations ($p \simeq 0.06$ and 0.02 , respectively), while the distribution of v_{md} is different ($p \approx 10^{-4}$). Matching the RL and RQ BALQ populations in the distribution of both He II EW and α_{UV} produces a similar distribution for both population in all three C IV BAL parameters. The K-S test results in $p \simeq 0.23$, 0.01 and 0.46 for v_{md} , FWHM and CF distribution, respectively, implying that these param-

ters are likely drawn from the same distributions for both RL and RQ BALQs.

3.2 Median BAL profiles – the quasar rest-frame versus the C IV BAL rest-frame

Figure 7 presents the median C IV and Si IV BAL profiles for the He II EW and α_{UV} bins. For a given bin, the median profile is evaluated by dividing the BALQ composite by the corresponding non-BALQ composite. The median profile is evaluated for two types of rest-frame. The first rest-frame is the quasar rest-frame (left panels), i.e. both BALQ and non-BALQ spectra are aligned based on z prior to calculating the composite (as done in BLH13). The second rest-frame is the rest-frame of the C IV BAL absorber (right panels), i.e. the BALQ spectra are aligned based on v_{md} , which is used to define $v_{shift} = 0$ (see Section 2). When calculating the non-BALQ composite, the non-BALQ spectra are shifted by v_{shift} that has the same distribution as v_{md} .

Fig. 7 presents a dramatic difference in the median C IV BAL profile between the two types of rest-frame. For the quasar rest-frame, the median BAL profile becomes broader by $\simeq 12,000 \text{ km s}^{-1}$ as the He II EW becomes weaker; and the absorption becomes deeper as α_{UV} becomes redder (as further discussed in BLH13). In contrast, for the C IV absorber rest-frame, the BAL profile remains narrow (FWHM $< 4000 \text{ km s}^{-1}$) for all bins; the FWHM of the median profile increases by only $\simeq 1000 \text{ km s}^{-1}$, from $\simeq 2500$ to 3500 km s^{-1} , as the He II EW decreases; and α_{UV} has only a small effect ($\simeq 15$ per cent) on the BAL CF. The CF increases from 0.7 to 0.8, both as α_{UV} becomes redder and as the He II EW decreases. The FWHM remains $\simeq 3000 \text{ km s}^{-1}$ for all α_{UV} bins. The large difference in the median profiles between the two rest-frames results from the dependence of the v_{md} distribution on the He II EW and α_{UV} (Fig. 3). In the bluer α_{UV} bins, v_{md} extends to higher velocities, compared to the redder bins. As a result, the individual C IV BAL profiles are spread over a larger range of velocities, yielding a shallower and broader median profile, although the individual profiles are nearly identical in the v_{md} frame. A similar effect takes place in the He II EW based bins.

It is interesting to note that the Si IV BAL absorption strength (seen at $v_{shift} \approx -30,000 \text{ km s}^{-1}$) increases significantly as the He II EW becomes weaker (Fig. 7, upper-right panel), with the median CF increasing from ~ 0.2 to ~ 0.5 . The Si IV doublet lines have a different absorption strength, indicating that the Si IV absorption is not fully saturated.

3.3 Comparison with previous studies

There are only a few studies which explore the distribution of properties of the C IV BAL profile in a large sample of BALQs. For a sample of BALQs from the SDSS DR5, Gibson et al. (2009) report that the total width of C IV BAL is typically smaller than 5000 km s^{-1} (fig. 9 there). This is consistent with the median FWHM being smaller than 4000 km s^{-1} for all He II EW and α_{UV} bins (Fig. 4). Gibson et al. (2009) also find that the distribution of v_{shift} reaches its maximum below $v_{shift} = 8000 \text{ km s}^{-1}$, and then gradually decreases with increasing v_{shift} . These findings are in accordance with the distribution of v_{md}

(Fig. 3). Allen et al. (2011) explore the distribution of the mean absorption depth of C IV BAL for BALQs from the SDSS DR6. They find that the distribution peaks at $\simeq 0.6$, which is roughly consistent with the maximum absorption of $\simeq 0.7 - 0.8$, implied by the composite profile in the absorber rest-frame (Fig. 7, right panels).

4 DISCUSSION

Why does the C IV absorption profile depend on the He II EW? As noted above (Section 1), the He II emission EW is likely an indicator of the hardness of the ionizing SED, since it measures the continuum strength above 54 eV relative to the near-UV continuum at $\lambda_{rest} = 1640 \text{ \AA}$. A higher value of He II EW corresponds to a harder SED, and vice-versa. This interpretation naturally explains the observed increase of Si IV BAL strength with decreasing He II EW (Fig. 7, upper-right panel). For a line-driven outflow, a softer SED implies a larger force multiplier for a given ionization state, and thus produces more favourable conditions for wind launching. A trend between the outflow v and the He II EW is implied by the mass flux continuity equation, i.e. $nv = \text{const.}$, where an outflow at a larger v has a lower density n . For a low enough n , the outflow becomes overionized and ceases to produce C IV absorption. For a softer ionizing SED (i.e. a weaker He II EW), overionization occurs at a lower n , and thus at a higher v .⁴ If the outflow is line driven, then the larger force multiplier for a softer SED results in a higher outflow velocity.

The interpretation of the He II EW as an indicator of the SED hardness can readily explain the observed trends. The interpretation implies that objects with a harder SED (a larger He II EW) will produce outflows with a smaller v_{md} and a narrower C IV BAL profile, as indeed observed (Figs 2–4). The BAL profile is narrower for a harder SED, since the gas that produces the absorption wings is already overionized at a higher n , and thus at a lower v . The interpretation is also consistent with the trend of the distribution of BAL CF with the He II EW (Fig. 5, left panels). The distribution has a tail of smaller values of BAL CF which increases as the He II EW becomes larger. The tail may represent a BALQ population with a non-saturated C IV absorption ($\tau \sim 1$), which is expected to be larger for a harder SED that can overionize larger columns of gas. Alternatively, the observed CF may be produced by the projected area of inhomogeneous gas clumps with $\tau \gg 1$ (Hamann et al. 2011). This area decreases for a harder SED, as the outer parts of the clumps become overionized, producing the observed tail of small values of CF.

Why does the C IV absorption profile depend on α_{UV} ? The value of α_{UV} is likely an indicator of our viewing angle, with a bluer α_{UV} indicating an angle closer to face-on. This interpretation assumes that α_{UV} is mostly set by reddening, and that the dust preferably resides in the symmetry plane of the quasar, i.e. the plane of the accretion disc (AD; see BLH13, section 5.2, for a detailed justification of this interpretation). The trend of the distribution of v_{md} with α_{UV} ,

⁴ The implied rise of the ionization parameter with v may also be produced by another mechanism (Fukumura et al. 2010a,b).

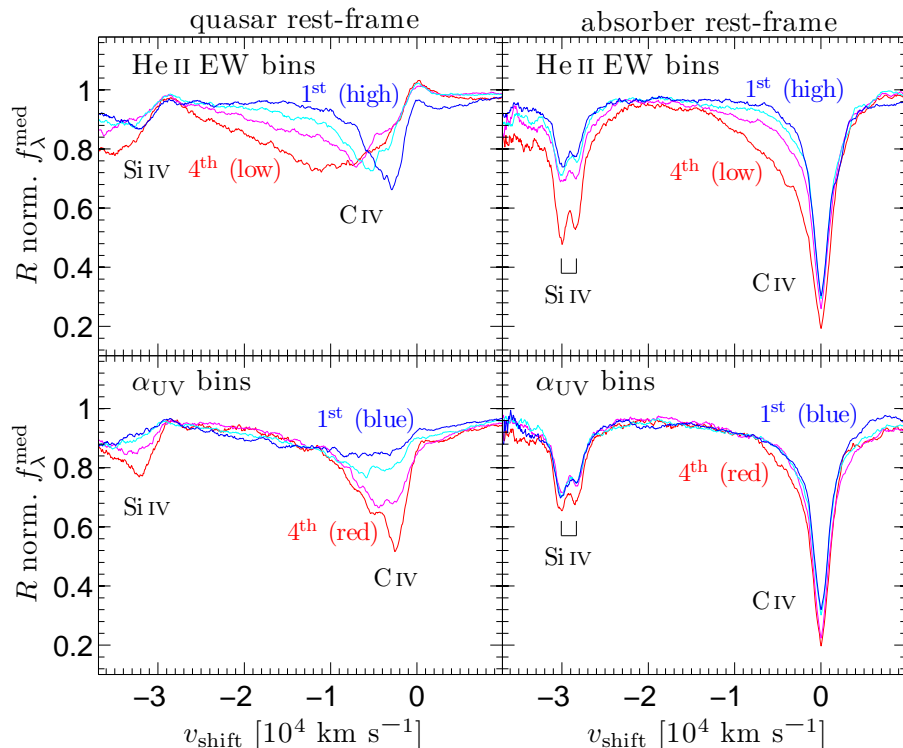


Figure 7. Comparison between the median C IV and Si IV BAL profiles in the quasar (left panels; an adaptation of fig. 9 of BLH13) and in the C IV absorber (right panels) rest-frame. The BAL profiles are presented for four bins of He II EW and for four bins of α_{UV} (top and bottom panels, respectively). The maximum depth of the C IV BAL profile in the absorber rest-frame is at $v_{\text{shift}} = 0$ by construction. For composites in the quasar rest-frame, the C IV BAL profile becomes broader and shifts to a higher v_{shift} , as the He II EW becomes lower; and the BAL profile becomes deeper as α_{UV} becomes redder. The FWHM of the median profile increases by $\simeq 12,000 \text{ km s}^{-1}$ from the highest to the lowest He II EW bin. The median BAL profile is broad ($\text{FWHM} \geq 5000 \text{ km s}^{-1}$) for all He II EW and α_{UV} bins. In contrast, for composites in the absorber rest-frame, the C IV BAL profile is narrow ($\text{FWHM} \leq 4000 \text{ km s}^{-1}$) for all bins; the FWHM of the median profile increases only by $\simeq 1000 \text{ km s}^{-1}$ from the highest to the lowest He II EW bin; and α_{UV} has only a small effect ($\simeq 15$ per cent) on the BAL depth. These differences are expected from the difference in the distribution of v_{md} and FWHM with the He II EW and α_{UV} (Figs 3 and 4). The Si IV BAL absorption that is associated with the C IV absorber increases as the ionizing SED becomes softer (i.e. a smaller He II EW; upper-right panel), as expected for a photoionized gas.

where there are more objects with a high v_{md} for a bluer α_{UV} (Fig. 3), may also be a viewing angle effect. This relationship between the acceleration and the viewing angle θ relative to the normal to the AD is expected, for example, for a line-driven outflow, since the driving UV continuum flux is expected to go as $\cos \theta$ for AD emission, and thus to produce a larger accelerating force for a smaller θ (see also Proga 2003; Kurosawa & Proga 2008).

The lack of a trend between the distribution of the C IV BAL FWHM and α_{UV} (Fig. 4), implies that the mechanism that produces the BAL velocity dispersion, as indicated by the absorption FWHM, is mostly isotropic and is independent of the bulk motion direction. It was recently reported by Hamann et al. (2013) for mini-BALs with extreme values of v_{md} that the absorbing gas may be in a form of a thin ‘pancake’-like filament. If this form also applies to regular BALs, as suggested by theoretical considerations (Baskin, Laor & Stern 2014b), then the BAL velocity dispersion probably originates from ordered motions which are internal to the filament and resemble turbulence.

The distribution of CF becomes bimodal for bluer α_{UV} slopes, and the bluest bin has two peaks, at $\text{CF} \simeq 0.9$ and 0.3 (Fig. 5). The peak at $\text{CF} \simeq 0.3$ may result from a larger

projected area of the emitting region for the blue (face-on) objects, which makes it harder for the outflow to cover the whole emitting region, compared to objects viewed edge-on. The typical BAL CF of $\simeq 0.7$ – 0.8 at maximum absorption (Fig. 7) may result from $\text{CF} \approx 1$ that is ‘diluted’ by scattered continuum from a medium with $\text{CF} \simeq 0.2$ – 0.3 , rather than from partial covering. A conclusive evidence for this scenario is provided by observations that find a high polarization level of the light at the bottom of the absorption troughs (Glenn, Schmidt & Foltz 1994; Cohen et al. 1995; Goodrich & Miller 1995; Ogle 1997; Schmidt & Hines 1999; Ogle et al. 1999; Lamy & Hutsemékers 2000, 2004; Brotherton, De Breuck & Schaefer 2006). The $\text{CF} \simeq 0.2$ – 0.3 required for the scattering medium is similar to the measured CF of 0.3 for the Broad Line Region (BLR; Korista et al. 1997b; Maiolino et al. 2001; Ruff et al. 2012). Thus, it is likely that the BLR is the scattering medium (Goodrich & Miller 1995; Korista & Ferland 1998), if the BAL outflow resides at a distance comparable to that of the BLR. The presence of significant structure within the BAL profile clearly demonstrates that it is not completely dominated by scattered light, which produces a trough with no structure.

The mass flux continuity likely explains the decrease in BAL CF with increasing v_{md} , which is observed for all bins of He II EW and α_{UV} (Fig. 6). The ionization level of the absorber increases with v_{md} , since the absorber n decreases with increasing v_{md} , from continuity. The increase of ionization level results in an overall drop in τ . Either $\tau < 1$ in a uniform absorber, or the CF of the part of the clumpy outflow with $\tau > 1$ becomes smaller.

The trends of the C IV BAL profile parameters with the He II EW and α_{UV} , which we find for HiBALQs, favour the scenario in which there is a smooth transition from HiBALQs to LoBALQs (e.g. Elvis 2000). LoBALQs are observed to have a redder continuum than HiBALQs (Weymann et al. 1991; Boroson & Meyers 1992; Sprayberry & Foltz 1992; Reichard et al. 2003; Gibson et al. 2009), and are likely predominantly located at the parameter-space of the lowest He II EW and the reddest α_{UV} (BLH13). The increase in the CF of C IV BAL with decreasing He II EW and redder α_{UV} (Fig. 5) implies that the C IV absorption in LoBALQs should be typically stronger than in HiBALQs, as indeed observed (Reichard et al. 2003; Allen et al. 2011; Filiz Ak et al. 2014). Allen et al. (2011) report that LoBALQs have a broader C IV BAL than HiBALQs. This is consistent with the increase of C IV BAL FWHM with decreasing He II EW (Fig. 4). The increase in the strength of the intermediate-ionization Si IV BAL with decreasing He II EW (Fig. 7) also favours the scenario of smooth transition between HiBALQs and LoBALQs.

4.1 Comparison between RL and RQ BALQs

Do RL BALQs differ in the C IV BAL properties from RQ BALQs? It has been suggested that RL BALQs have different BAL properties compared to RQ BALQs (e.g. Becker et al. 1997; Brotherton et al. 1998; cf. Rochais et al. 2014). We find that this difference does not result from radio loudness, but rather from the preference of RL BALQs to have a weak He II EW and a red α_{UV} (Fig. 1, and Tables 2 and 3; see also Rochais et al. 2014, fig. 6 there). When RL and RQ BALQs are matched in the He II EW and α_{UV} , both subclasses show similar C IV BAL properties (Section 3.1.1; see also Figs 2 and 6). Richards et al. (2011) reach a similar conclusion for the broad emission lines. They match RL and RQ non-BALQs by luminosity, z and the C IV emission EW and blueshift, and find no significant difference in other emission lines between the two subclasses. As we show below, the C IV emission EW and blueshift have a strong correlation with the He II EW (see also Baskin, in preparation).

RL non-BALQs have a higher He II EW and a bluer α_{UV} compared to RL BALQs, similarly to the RQ subclass (Tables 2 and 3). However, RL non-BALQs are redder than RQ non-BALQs. The median α_{UV} is -0.84 for RL non-BALQs and -0.69 for RQ non-BALQs; and 23 per cent of RL non-BALQs reside in the reddest bin, compared to only 11 per cent of RQ non-BALQs. In contrast, the median He II EW is similar for both RL and RQ non-BALQ populations (5.4 and 5.1 Å, respectively), and both populations are similarly distributed among the He II EW bins.

The observed BALQ fraction from the total RL quasar population increases from 4 (4) per cent in the highest He II EW (bluest α_{UV}) bin to 28 (21) per cent in the lowest He II EW (reddest α_{UV}) bin. The complete quasar sample, which

is dominated by RQ quasars ($\simeq 94$ per cent of BALQs and non-BALQs), produces a comparable observed BALQ fraction in the corresponding bins (BLH13; see also Section 2). This further supports the suggestion that radio-loudness does not directly affect BAL properties.

The preference of RL BALQs to lie in the parameter-space of weak He II EW and red α_{UV} explains the large fraction of LoBALQs in RL BALQ samples, as LoBALQs have preference for the same parameter-space (see above). Becker et al. (2000) find a LoBALQ fraction of $\simeq 0.5$ in the FIRST BALQ sample, compared to ~ 0.1 found in SDSS samples that are dominated by RQ BALQs. DiPompeo et al. (2011) report that RL BALQs are typically viewed at larger angles relative to the radio-jet axis compared to RL non-BALQs. This supports the interpretation of α_{UV} as an inclination angle indicator, where a redder α_{UV} implies a larger angle, since the radio-jet axis is likely to be perpendicular to the symmetry plane of the system.

4.2 Similar relations for the Broad Line Region C IV emission

There are observational indications that the BLR emission originates in two components, a disc and a wind component (Collin-Souffrin et al. 1988; Wills et al. 1993; Leighly & Moore 2004; Richards et al. 2011; Kruczek et al. 2011). Recently, Baskin et al. (2014b) noted that if the BAL gas is located at distances similar to those of the BLR, then it likely contributes to the emission of broad lines. This BAL gas may very well be the optically-thin BLR gas that was suggested by Shields, Ferland & Peterson (1995). Does the wind component of the BLR show similar trends to those of BAL outflows?

Figure 8 presents the C IV emission-line profile for the *non-BALQ* bins of He II EW and α_{UV} . The same non-BALQ bins from the BAL analysis are adopted (i.e. the non-BALQ sample is not rebinned), and the plotted C IV profiles correspond to the unabsorbed C IV emission of matching BALQ bins. The C IV emission becomes weaker and more blueshifted and asymmetric as the He II EW becomes weaker (Fig. 8, top panel). This trend results from the transition of C IV emission from being dominated by the disc component (high He II EW objects) to being dominated by the wind component (low He II EW objects). A similar trend is presented in Richards et al. (2011, fig. 11 there). The total C IV emission decreases with a decreasing He II EW, since the dominant emitter of C IV is the disc component, which is likely radiation bounded. As the SED becomes softer (lower He II EW), the production of C^{3+} decreases for a radiation-bounded gas, and the C IV emission EW becomes lower (e.g. Baskin, Laor & Stern 2014a). Radiation-bounded gas absorbs all of the ionizing radiation, and thus the line emission should be stronger for a harder SED that has more ionizing photons, as observed (Fig. 8, top panel). A similar trend of decreasing C IV emission with a decreasing He II EW is observed for the red wing of C IV in BALQs (BLH13). The C IV emission from the wind component is marginally stronger for a softer SED (lower He II EW; Baskin, in preparation), since this component is likely matter bounded. As the SED becomes softer, a matter-bounded wind ($\tau < 1$) produces C^{3+} down to a lower n , and yields C IV emission that extends up to a higher v_{shift} (from mass flux continu-

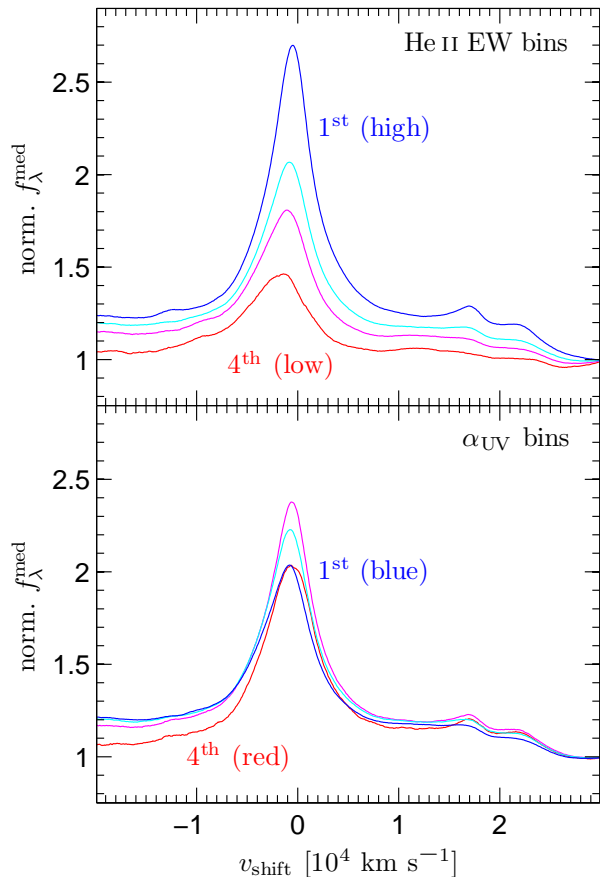


Figure 8. The dependence of the C IV emission-line profile of *non-BALQs* on the He II EW and α_{UV} (top and bottom panel, respectively). The He II EW affects both the C IV strength and shape. As the He II EW becomes weaker, the C IV emission becomes weaker, more blue-shifted and more asymmetric. For the first three α_{UV} bins, the C IV emission becomes stronger as α_{UV} becomes redder.

ity), as observed. The relation between the total C IV line emission from the wind and the SED depends on the wind density structure, and requires detailed calculations. A possible connection between the BLR wind component and the BAL outflow will be addressed in a future study (Baskin, in preparation).

The trend of C IV emission with α_{UV} is consistent with α_{UV} being an indicator of our viewing angle. The C IV EW becomes larger for a redder α_{UV} for the first three bins, and then decreases for the fourth reddest bin (Fig. 8, bottom panel; note that all composites are normalized to 1 at $\lambda_{rest} = 1700 \text{ \AA}$). The BLR emission is likely only weakly dependent on inclination θ . In contrast, the underlying UV continuum from the AD goes as $\cos \theta$. The combined effect results in a decrease of the continuum flux relative to the C IV flux, i.e. an increase of the C IV EW, as the inclination angle gets closer to edge-on (i.e. a redder α_{UV}). The trend of increasing C IV EW with a redder α_{UV} is consistent with Richards et al. (2002).

Our findings (Fig. 8) are consistent with the correlations reported by Baskin & Laor (2005) for a complete and well defined sample of Palomar-Green quasars (Boroson & Green 1992). The reported correlation between α_{ox} and the C IV

EW (see also Kruczek et al. 2011) is consistent with C IV becoming weaker for a lower He II EW. The anti-correlation between the optical-UV slope and the C IV EW is consistent with C IV becoming stronger with a redder α_{UV} . The anti-correlation between the C IV blueshift and its EW (see also Richards et al. 2002, 2011) is detected here for both the He II EW and α_{UV} binning. We leave the full analysis of the non-BALQ sample to a separate study (Baskin, in preparation).

The range of He II EW values for objects in our sample (Fig. 1) can be produced by the observed range of ionizing SED slopes (i.e. α_{ion} from -2.0 to -1.2 , where α_{ion} is defined between $\lambda_{rest} = 912$ and 12 \AA ; Baskin et al. 2014a, fig. 5 there). A relation between the He II EW and the SED may be indicated by the strong relation of He II EW with the quasar luminosity L (Boroson & Green 1992; Dietrich et al. 2002), and the relation between L and the SED (Scott et al. 2004; Strateva et al. 2005; Steffen et al. 2006; Just et al. 2007; Stern & Laor 2012; cf. Telfer et al. 2002; Shull et al. 2012). Korista, Ferland & Baldwin (1997a) suggested that the BLR does not see the same SED we do. They adopt a baseline of 0.1 for the BLR CF, and use the Locally Optimally emitting Cloud (LOC) model of the BLR, where a single slab of gas produces line emission from a rather limited range of ionization states (Baldwin et al. 1995). However, adopting the observed BLR CF of $\simeq 0.3$ (see above), and noting that a single slab produces line emission from a very broad range of ionization states (Baskin et al. 2014a), alleviate the need in a different SED for the BLR. The interpretation of He II EW as an indicator of SED hardness can be directly tested by observations that cover the extreme-UV range (e.g. Stevans et al. 2014).

5 CONCLUSIONS

We analyse the distribution of the C IV BAL profiles for a sample of BALQs from the SDSS DR7, which covers the wavelength range of $1400\text{--}3000 \text{ \AA}$. In contrast with our earlier study (BLH13), where we explored the median absorption profile in the quasar emission frame, here we present the median absorption profile in the outflow frame, defined by the velocity at maximum depth of absorption. The median absorption profile in the absorber frame is quite different from the median in the quasar emission frame. We find the following:

- (i) Although the typical wind velocity is $v_{md} \simeq 6500 \text{ km s}^{-1}$, the velocity dispersion is small, with a median FWHM = 3500 km s^{-1} . Only 4 per cent of BALQs have FWHM $> 10,000 \text{ km s}^{-1}$.
- (ii) The He II emission-line EW affects the distribution of the wind velocity dispersions. The distribution peaks at FWHM $< 3000 \text{ km s}^{-1}$, and decreases approximately as a power law at FWHM $> 3000 \text{ km s}^{-1}$. The power law slope is flat (-1.1) when the He II EW is low ($\simeq 1 \text{ \AA}$), and steep (-2.5) when the EW is high ($\simeq 7 \text{ \AA}$). In contrast, the FWHM distribution is not affected by the α_{UV} slope.
- (iii) The wind outflow velocity extends to higher values of v_{md} as the He II EW decreases, from a median value of v_{md} of 5200 km s^{-1} for EW $\simeq 7 \text{ \AA}$, to a median value of 8000 km s^{-1} for EW $\simeq 1 \text{ \AA}$. The outflow velocity extends to higher values also for a bluer α_{UV} , from 4500 km s^{-1} for $\alpha_{UV} \simeq -1.5$, to 8700 km s^{-1} for $\alpha_{UV} \simeq -0.5$.

(iv) The distribution of the wind CF increases from $CF = 0$ as $\propto CF^{1.6}$, and peaks at $CF = 0.9$. The distribution does not depend on either the He II EW or α_{UV} . There is an additional component which contributes only at the $CF < 0.5$ range, and its contribution is larger for a higher He II EW and a bluer α_{UV} .

(v) Radio-loud BALQs have similar outflow properties to RQ BALQs when the two subclasses are matched in the He II EW and α_{UV} . The reported difference in BAL properties between RL and RQ BALQs results from the preference of RL BALQs to have a smaller He II EW and a redder α_{UV} compared to RQ BALQs.

(vi) The C IV emission line of *non-BALQs* also shows trends with the He II EW and α_{UV} . The symmetric C IV emission, which is attributed to the ‘disc component’ of the BLR, decreases with decreasing He II EW. The line becomes more asymmetric and blueshifted as the He II EW decreases. The line EW increases with increasing reddening, while its velocity profile is roughly independent of α_{UV} .

The trends with the He II EW described above are consistent with the interpretation that the He II EW is an indicator of the hardness of the ionizing SED (extreme-UV relative to far-UV). For a softer SED (a lower He II EW), the BAL outflow extends to a lower n , and thus to a higher v (from mass flux continuity), producing C IV BAL profiles that are broader, and have a higher v_{shift} and a larger CF, as observed. The trends with α_{UV} are consistent with the interpretation that α_{UV} is an indicator of our viewing angle θ . For a viewing angle closer to face-on (a bluer α_{UV}), the AD continuum flux that goes as $\cos \theta$ is larger, and a line-driven wind can be accelerated to larger velocities, as observed. For this viewing angle, the emitting region has a larger projected area, which makes it harder for the outflow to fully cover the emitting region, and produces BALs with $CF < 0.5$. The mechanism that sets the BAL FWHM is likely independent of the viewing angle.

As pointed out in BLH13, the interpretation of α_{UV} as an indicator of viewing angle can be tested by searching for a relationship between α_{UV} and the continuum polarization, in both non-BALQs and BALQs. This interpretation also implies a trend between α_{UV} and the X-ray absorbing column, which can be looked for. Spectra from the Cosmic Origins Spectrograph on board the Hubble Space Telescope, which cover the wavelength range of $\simeq 500\text{--}2000$ Å (Stevens et al. 2014), can be utilized to directly test the interpretation of the He II EW as an indicator of the SED hardness.

ACKNOWLEDGEMENTS

We thank the anonymous referee and G. Richards for valuable comments and suggestions. This research was supported by the Israel Science Foundation (grant No. 1561/13). This research has made use of the Sloan Digital Sky Survey which is managed by the Astrophysical Research Consortium for the Participating Institutions; and of NASA’s Astrophysics Data System Bibliographic Services.

Funding for the SDSS and SDSS-II has been provided by the Alfred P. Sloan Foundation, the Participating Institutions, the National Science Foundation, the U.S. Department of Energy, the National Aeronautics and Space

Administration, the Japanese Monbukagakusho, the Max Planck Society, and the Higher Education Funding Council for England. The SDSS Web Site is <http://www.sdss.org/>.

The SDSS is managed by the Astrophysical Research Consortium for the Participating Institutions. The Participating Institutions are the American Museum of Natural History, Astrophysical Institute Potsdam, University of Basel, University of Cambridge, Case Western Reserve University, University of Chicago, Drexel University, Fermilab, the Institute for Advanced Study, the Japan Participation Group, Johns Hopkins University, the Joint Institute for Nuclear Astrophysics, the Kavli Institute for Particle Astrophysics and Cosmology, the Korean Scientist Group, the Chinese Academy of Sciences (LAMOST), Los Alamos National Laboratory, the Max-Planck-Institute for Astronomy (MPIA), the Max-Planck-Institute for Astrophysics (MPA), New Mexico State University, Ohio State University, University of Pittsburgh, University of Portsmouth, Princeton University, the United States Naval Observatory, and the University of Washington.

REFERENCES

- Abazajian K. N. et al., 2009, *ApJS*, 182, 543
- Adelman-McCarthy J. K. et al., 2007, *ApJS*, 172, 634
- Adelman-McCarthy J. K. et al., 2008, *ApJS*, 175, 297
- Allen J. T., Hewett P. C., Maddox N., Richards G. T., Belokurov V., 2011, *MNRAS*, 410, 860
- Baldwin J., Ferland G., Korista K., Verner D., 1995, *ApJ*, 455, L119
- Baskin A., Laor A., 2005, *MNRAS*, 356, 1029
- Baskin A., Laor A., Hamann F., 2013, *MNRAS*, 432, 1525 (BLH13)
- Baskin A., Laor A., Stern J., 2014a, *MNRAS*, 438, 604
- Baskin A., Laor A., Stern J., 2014b, *MNRAS*, 445, 3025
- Becker R. H., White R. L., Helfand D. J., 1995, *ApJ*, 450, 559
- Becker R. H., Gregg M. D., Hook I. M., McMahon R. G., White R. L., Helfand D. J., 1997, *ApJ*, 479, L93
- Becker R. H., White R. L., Gregg M. D., Brotherton M. S., Laurent-Muehleisen S. A., Arav N., 2000, *ApJ*, 538, 72
- Boroson T. A., Green R. F., 1992, *ApJS*, 80, 109
- Boroson T. A., Meyers K. A., 1992, *ApJ*, 397, 442
- Brandt W. N., Laor A., Wills B. J., 2000, *ApJ*, 528, 637
- Brotherton M. S., van Breugel W., Smith R. J., Boyle B. J., Shanks T., Croom S. M., Miller L., Becker R. H., 1998, *ApJ*, 505, L7
- Brotherton M. S., De Breuck C., Schaefer J. J., 2006, *MNRAS*, 372, L58
- Cohen M. H., Ogle P. M., Tran H. D., Vermeulen R. C., Miller J. S., Goodrich R. W., Martel A. R., 1995, *ApJ*, 448, L77
- Collin-Souffrin S., Dyson J. E., McDowell J. C., Perry J. J., 1988, *MNRAS*, 232, 539
- Dietrich M., Hamann F., Shields J. C., Constantin A., Vestergaard M., Chaffee F., Foltz C. B., Junkkarinen V. T., 2002, *ApJ*, 581, 912
- DiPompeo M. A., Brotherton M. S., De Breuck C., Laurent-Muehleisen S., 2011, *ApJ*, 743, 71
- Elvis M., 2000, *ApJ*, 545, 63
- Filiz Ak N., et al., 2014, *ApJ*, 791, 88

- Fukumura K., Kazanas D., Contopoulos I., Behar E., 2010a, *ApJ*, 715, 636
- Fukumura K., Kazanas D., Contopoulos I., Behar E., 2010b, *ApJ*, 723, L228
- Gibson R. R. et al., 2009, *ApJ*, 692, 758
- Glenn J., Schmidt G. D., Foltz C. B., 1994, *ApJ*, 434, L47
- Goodrich R. W., Miller J. S., 1995, *ApJ*, 448, L73
- Hamann F., Korista K. T., Morris, S. L., 1993, *ApJ*, 415, 541
- Hamann F., Kanekar N., Prochaska J. X., Murphy M. T., Ellison S., Malec A. L., Milutinovic N., Ubachs W., 2011, *MNRAS*, 410, 1957
- Hamann F., Chartas G., McGraw S., Rodriguez Hidalgo P., Shields J., Capellupo D., Charlton J., Eracleous M., 2013, *MNRAS*, 435, 133
- Hewett P. C., Foltz C. B., 2003, *AJ*, 125, 1784
- Hewett P. C., Wild V., 2010, *MNRAS*, 405, 2302
- Junkkarinen V. T., Burbidge E. M., Smith H. E., 1983, *ApJ*, 265, 51
- Just D. W., Brandt W. N., Shemmer O., Steffen A. T., Schneider D. P., Chartas G., Garmire G. P., 2007, *ApJ*, 665, 1004
- Korista K., Ferland G., 1998, *ApJ*, 495, 672
- Korista K., Ferland G., Baldwin J., 1997a, *ApJ*, 487, 555
- Korista K., Baldwin J., Ferland G., Verner D., 1997b, *ApJS*, 108, 401
- Knigge C., Scaringi S., Goad M. R., Cottis C. E., 2008, *MNRAS*, 386, 1426
- Kruczek N. E., Richards G. T., Gallagher S. C., Deo R. P., Hall P. B., Hewett P. C., Leighly K. M., Krawczyk C. M., Proga D., 2011, *AJ*, 142, 130
- Kurosawa R., Proga D., 2008, *ApJ*, 674, 97
- Lamy H., Hutsemékers D., 2000, *A&A*, 356, L9
- Lamy H., Hutsemékers D., 2004, *A&A*, 427, 107
- Laor A., Brandt W. N., 2002, *ApJ*, 569, 641
- Leighly K. M., Moore J. R., 2004, *ApJ*, 611, 107
- Maddox N., Hewett P. C., Warren S. J., Croom S. M., 2008, *MNRAS*, 386, 1605
- Maiolino R., Salvati M., Marconi A., Antonucci R. R. J., 2001, *A&A*, 375, 25
- Ogle P. M., 1997, *ASPC*, 128, 78
- Ogle P. M., Cohen M. H., Miller J. S., Tran H. D., Goodrich R. W., Martel A. R., 1999, *ApJS*, 125, 1
- Pâris I. et al., 2011, *A&A*, 530, A50
- Proga D., 2003, *ApJ*, 585, 406
- Reichard T. A., Richards G. T., Hall P. B., Schneider D. P., Vanden Berk D. E., Fan X., York D. G., Knapp G. R., Brinkmann, J., 2003, *AJ*, 126, 2594
- Richards G. T., Vanden Berk D. E., Reichard T. A., Hall P. B., Schneider D. P., SubbaRao M., Thakar A. R., York D. G., 2002, *AJ*, 124, 1
- Richards G. T., et al., 2011, *AJ*, 141, 167
- Rochais T. B., DiPompeo M. A., Myers A. D., Brotherton M. S., Runnoe J. C., Hall S. W., 2014, *MNRAS*, 444, 2498
- Ruff A. J., Floyd D. J. E., Webster R. L., Korista K. T., Landt H., 2012, *ApJ*, 754, 18
- Shields J. C., Ferland G. J., Peterson B. M., 1995, *ApJ*, 441, 507
- Schmidt G. D., Hines D. C., 1999, *ApJ*, 512, 125
- Schneider D. P. et al., 2010, *AJ*, 139, 2360
- Scott J. E., Kriss G. A., Brotherton M., Green R. F., Hutchings J., Shull J. M., Zheng W., 2004, *ApJ*, 615, 135
- Shen Y., Greene J. E., Strauss M. A., Richards G. T., Schneider D. P., 2008, *ApJ*, 680, 169
- Shen Y. et al., 2011, *ApJS*, 194, 45
- Shull J. M., Stevans M., Danforth C. W., 2012, *ApJ*, 752, 162
- Sprayberry D., Foltz C. B., 1992, *ApJ*, 390, 39
- Steffen A. T., Strateva I., Brandt W. N., Alexander D. M., Koekemoer A. M., Lehmer B. D., Schneider D. P., Vignali C., 2006, *AJ*, 131, 2826
- Stern J., Laor A., 2012, *MNRAS*, 423, 600
- Stevans M. L., Shull J. M., Danforth C. W., Tilton E. M., 2014, *ApJ*, 794, 75
- Strateva I. V., Brandt W. N., Schneider D. P., Vanden Berk D. G., Vignali C., 2005, *AJ*, 130, 387
- Telfer R. C., Zheng W., Kriss G. A., Davidsen A. F., 2002, *ApJ*, 565, 773
- Turnshek D. A., Grillmair C. J., Foltz C. B., Weymann R. J., 1988, *ApJ*, 325, 651
- Vestergaard M., Osmer P. S., 2009, *ApJ*, 699, 800
- Weymann R. J., Carswell R. F., Smith M. G., 1981, *ARA&A*, 19, 41
- Weymann R. J., Morris S. L., Foltz C. B., Hewett P. C., 1991, *ApJ*, 373, 23
- White R. L., Becker R. H., Helfand D. J., Gregg M. D., 1997, *ApJ*, 475, 479
- Wills B. J., Brotherton M. S., Fang D., Steidel C. C., Sargent W. L. W., 1993, *ApJ*, 415, 563
- York D. G. et al. 2000, *AJ*, 120, 1579

This paper has been typeset from a \LaTeX file prepared by the author.